Critical Review Vol. CR38, Infrared Optical Design and Fabrication, ed. R. Hartmann, W.J. Smith (Apr 1991) Copyright SPIE

Diamond Windows for the Infrared: Fact and Fallacy

Claude A. Klein
Raytheon Company, Research Division
Lexington, MA 02173

ABSTRACT

Diamond exhibits an unusually favorable combination of properties in terms of mechanical strength, thermal conductivity, and optical transmission, which makes this material highly attractive for infrared (IR) applications that involve severe environmental conditions. Until recently, diamond has been available only in the form of relatively small crystals, but this situation is evolving rapidly as a result of major advances in the art of growing diamond by low-pressure chemical vapor deposition (CVD) techniques. Success in producing large, free-standing deposits with properties that match those of natural diamond has stimulated enormous interest and has given rise to much speculation about CVD diamond as an "ideal" optical material for a wide range of engineering uses in the IR: there are, however, limiting factors that must be taken into consideration. The objective of this *Critical Review* is to provide an initial assessment of some of the issues that arise in connection with the use of diamond artifacts for two highly demanding tasks: domes for high-speed missiles and windows for high-power lasers.

Monolithic diamond deposits lack the degree of transparency required for operation as transmissive optics elements in the mid-IR: at longer wavelengths (LWIR), it can be reasonably expected that single-phonon absorptions will be tolerable in the sense that self-emission phenomena at elevated temperatures should not be catastrophic. Besides surface hardness, the features that confer diamond its advantage are the high thermal conductivity and the low thermal expansion, which indicate that diamond has orders of magnitude more thermal shock resistance than some of the best competing materials. There is little doubt that the "new diamond" technology will provide a credible, if not outstanding LWIR dome material for tactical missiles operating at speeds up to but not beyond Mach 4 in the atmosphere.

Defect-free, single-crystal diamond also emerges as a promising candidate material for high-average-power laser window applications in the near-IR. The power-handling capability (<1 MW independently of the window size) will be limited by (a) thermally induced optical distortion, which can only be eliminated if absorption-free anti-reflection coatings become available, and (b) the edge heat-transfer coefficient, which must be greatly enhanced to take advantage of the exceptional thermal conductivity of diamond at low temperatures. Pressure-induced and thermally-induced stresses are of no consequence, but peak laser intensities in excess of, say 1 GW/cm^2 should be avoided because of unfavorable non-linear refractive index characteristics.

1. INTRODUCTION

Diamond has a cubic lattice structure and a very wide bandgap, which is often interpreted as indicative of "excellent" optical transparency from the far infrared to the near ultraviolet. Since diamond also exhibits unusually favorable properties from the point of view of mechanical hardness, chemical stability, and thermal conductivity, there is considerable interest in this material for infrared (IR) applications that may involve severe environmental conditions. Indeed, diamond windows have been used in the context of space-related activities such as the *Pioneer Venus* probe, whose purpose it was to perform planetary radiometric measurements in five spectral bands ranging from 3 to 40 μm.[1] This spectral range encompasses the region of two- and three-phonon absorptions (2.5 to 7.5 μm) first described by Hardy and Smith,[2] which degrade the IR transmittance of natural as well as synthetic diamond crystals, including the type IIa's: implications of this situation, particularly in terms of potential missile-dome applications for the mid-IR, have not always been properly taken into consideration. Furthermore, since most diamonds contain impurities and show evidence of lattice disorder, their optical properties are not those of perfect 3C crystals, which suggests that first-order (single-phonon) processes may occur, thus generating IR absorption in the 10-μm wavelength region, as first demonstrated more than thirty years ago.[3]

Until recently, diamond has been available only in the form of relatively small crystals; this state of affairs is changing rapidly as a result of major advances in the science of growing diamond by low-pressure chemical vapor deposition (CVD) techniques. In fact, it has been said that the successful deposition of diamond on a variety of large-area substrates, at acceptable growth rates, represents one of the most significant technological developments of the past decade.[4] It provides, in particular, an opportunity to exploit many of the exceptional features of this material for applications that require "good" transparency in the infrared. The research community concerned with "diamond for the infrared" is now expanding rapidly and, undoubtedly, will succeed in developing diamond into an optical material that possesses greatly enhanced environmental damage as well as thermal shock resistance. This includes[5] not only erosion-resistant protective coatings on well-established IR window materials but also free-standing diamond components that can handle extreme thermal or thermo-mechanical loads; in practical terms, success amounts to demonstrating

the feasibility of high-growth-rate deposition processes[6] while mitigating the impact of IR absorption mechanisms alluded to earlier. For orientation purposes, I will briefly consider those applications where the availability of affordable, well-crystallized CVD diamond may lead to important advances with regard to contemplated IR systems for military purposes.

(a) Zinc sulfide is currently the long-wavelength infrared (LWIR) material of choice for less-demanding applications such as windows for airborne forward-looking infrared (FLIR) imaging systems. These windows lack the desired resistance to rain and dust erosion, but CVD-diamond coatings may provide the "ultimate" solution if IR-transparent films of adequate thickness can be deposited on ZnS. The central difficulty revolves about the issue of high substrate temperatures (> 600°C), since the differential contraction that takes place subsequent to the deposition generates large shear stresses and, hence, may cause delaminations; this problem already has been examined in some detail[7] and will not be dealt with in this paper.

(b) Air-launched tactical missiles as well as ground-launched missile interceptors presently in concept development will be operating at supersonic/hypersonic speeds that far exceed present levels; furthermore, they will require IR guidance modules for terminal homing.[8] At present, there are no available LWIR materials that can handle the anticipated thermal load without catastrophic failure of the aerodynamic dome or the sensor window depending upon the system configuration. In terms of the conventional figure of merit for thermal shock,*

$$R' = \frac{\sigma_f (1-\nu) k}{\alpha E} , \qquad (1)$$

hard monolithic diamond should provide orders of magnitude of improvement, which strongly suggests that future requirements will be met if fine-grained, high-purity diamond crystalline structures can be produced.

---

* The notations are as specified in the Appendix.

(c) In addition to "low-power" optical applications, *i.e.*, IR transmitting windows for passive guidance systems, diamond is also being promoted as a material candidate for components that must function in the high-photon-flux environment of free-electron lasers.[9] At first glance, properties such as low expansion coefficient and unsurpassed thermal conductivity point to exceptional power-handling capabilities, particularly at lower temperatures, but it would indeed be surprising if diamond did not have some disadvantages; the most serious one relates to the thermo-optic coefficient, dn/dT, as discussed in Sec. 4. At this point, we should also emphasize that any diamond laser-window application as presently envisioned rests on the feasibility of growing defect-free single crystals in sizes way beyond the state of the art.

The enormous potential of diamond as an IR transmitting material has stimulated considerable interest, primarily because of the continuing need to search for and develop optical materials that possess "ideal" properties. Diamond has many advantages and has been promoted as the "ultimate" optical material[10]; there are, however, limiting factors that must be taken into consideration. The objective of this *Critical Review* is to provide an initial assessment of the issues that arise in connection with using large synthetic diamonds for two highly demanding tasks, namely domes for high-speed missiles and windows for high-power lasers. For that purpose, I will first review (Sec. 2) the relevant properties of diamond and select two specific items for additional discussion: the spectral absorption features in the IR and the intrinsic anisotropy of diamond elasticity. In Sec. 3, I propose to evaluate how diamond domes perform on postulated air-to-air missile trajectories and to demonstrate that the thermostructural capability of such domes far exceeds present requirements; operation at high speeds/high temperatures, however, imposes limits on the tolerable IR absorption to prevent "blinding" the detectors. Issues relating to the distortion- and the damage-free transmission of very powerful laser beams through diamond windows will be addressed in Sec. 4, where it will be shown that, while cooling greatly enhances the power-handling capability, it cannot compensate for limitations caused by unfavorable refractive-index characteristics. Finally, the conclusions are stated in Sec. 5.

2. PHYSICAL PROPERTIES OF DIAMOND

At present, the vapor-growth process of diamond appears to be handicapped by poorly controlled formation of independent diamond nuclei during the early phases of the deposition: this leads to polycrystalline structures with typical grain sizes of approximately 10 μm and surfaces that are faceted as illustrated in Fig. 1. Many of the deposits are highly oriented, the (110) planes growing preferentially parallel to the substrate surface, and show evidence for the presence of non-crystalline carbon phases at the grain boundaries.[5] Nevertheless, the properties of these CVD diamonds are not significantly different from those of single-crystal natural diamond, even for morphologies that are fine grained with no distinguishable faceting. The mechanical, thermal, and optical properties that relate directly to the performance of diamond as an infrared-transmitting material are summarized in Sec. 2.1. The transparency in the infrared warrants further discussion because of its unusual features and the controversy about IR-active modes in the one-phonon region (Sec. 2.2). Also, the polycrystalline nature of CVD diamond affects the elastic properties, which requires some clarification and, in particular, a proper assessment of the effect of anisotropic elastic constants on Young's modulus and Poisson's ratio (Sec. 2.3).

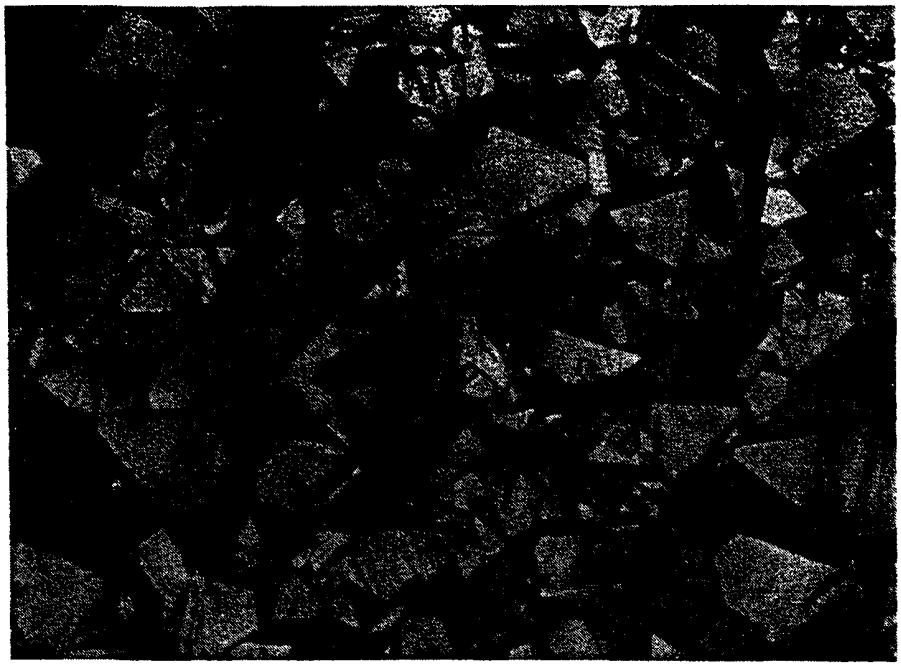

Fig. 1. Reflected-light micrograph of a CVD-diamond specimen prepared at Raytheon Company.

2.1. List of Properties

The property values I made use of in this evaluation of diamond as a window/dome material are listed in Table 1. With the exception of the tensile strength.[11] these numbers originate from readily available compilations,[12,13] where the reader may find references to source literature; the numbers also apply to CVD diamond taking into consideration that, to some extent, the properties depend on the "quality" of the deposit. Rather than attempting to review the body of data already available, I will confine myself to commenting about the mechanical strength, the thermal conductivity, and the refractive index of diamond.

Table 1. Mechanical, thermal, and optical properties of diamond

Mass density:	$\rho = 3.52\ gcm^{-3}$		Ref. 12
Elastic Constants:	$s_{11} = 0.953\ TPa^{-1}$		Ref. 12
	$s_{12} = -0.099$ -		
	$s_{44} = 1.744$ -		
Tensile Strength:	$\sigma_f = 406$ kpsi		Ref. 11
Thermal Expansion:	$\alpha = 1\times10^{-6}\ K^{-1}$	at 293 K	Ref. 12
	$= 5\times10^{-8}$ -	- 110 K	
Thermal Conductivity:	$k = 6.6\ Wcm^{-1}K^{-1}$	at 273 K	Ref. 12
	=34.0 -	- 77 K	
Specific Heat:	$C_p = 5.1\times10^{-1}\ Jg^{-1}K^{-1}$	at 298 K	Ref. 12
	$= 5.6\times10^{-3}$ -	- 70 K	
Optical Bandgap:	$\varepsilon_G = 5.4$ eV		Ref. 12
Refractive Index:	$n = 2.418$	at 0.589 μm	Ref. 13
	= 2.376	- 10.0 μm	
Thermo-Optic Coeff.:	$dn/dT = 1\times10^{-5}K^{-1}$		Ref. 13

(a) The measured strength of single-crystal diamond specimens is of the order of 400 kpsi (2.8 GPa), or roughly one fiftieth of the theoretical strength,[11] which points to the overwhelming effect of lattice flaws in this material. The few available data points for CVD-diamond films[14] (tensile stress at rupture) cover a wide range as expected of brittle material, but their average, $\bar{\sigma}_f$=436 kpsi, turns out to be surprisingly close to the reported value for natural diamond. If this is indeed more than a coincidence, it would appear that, in terms of strength, diamond does not match the graphite fibers used in filament-wound structures, which have tensile strengths of 1.3 Mpsi.

(b) At room temperature, diamond possesses the highest thermal conductivity of any known material, and recent work has shown that further enhancement can be brought about by chemically vapor-depositing isotopically pure cubic ^{12}C.[15] Below room temperature, the thermal conductivity may increase quite substantially (see Table 1), presumably because of the reduced rate of *Umklapp* processes, but this has not yet been observed with CVD specimens.[4] Still, since many of the contemplated applications of synthetic diamond rely heavily on "heat superconductivity" at liquid nitrogen temperatures, it may not be unrealistic to set k equal to 34 W/(cmK) for evaluating the performance of edge-cooled diamond laser windows (see Sec. 4).*

(c) The refractive index of diamond is rather high ($n \approx 2.40$), which some authors consider to be a serious limitation.[16] Actually, the single-surface reflectivity, $(n-1)^2/(n+1)^2$, amounts to 17%, which implies that, in the absence of internal losses, a polished diamond dome may transmit as much as 83% of the incident light if the inner surface has been properly coated. Anti-reflection (AR) coatings on the outer surface would be desirable but they may well nullify the rain-erosion resistance advantage of using diamond and, therefore, are probably of questionable utility under severe environmental conditions.

---

* Thermal conductivities as high as 28 W/(cmK), below room temperature, have now been reported for microwave-plasma assisted CVD diamond (C. Robinson, Raytheon Co., private communication).

2.2. Infrared Absorption

Some of the early discussions of CVD diamond as an IR material (see, for instance, Ref. 17) attribute "almost" all absorption to impurities and infer that pure synthetic material will have a very low absorption coefficient. To support such speculations, it has been argued that the triply-degenerate fundamental lattice mode at 1333 cm^{-1} (7.5 μm) should be IR inactive due to symmetry considerations and, further, that second-order (two-phonon) intrinsic absorptions should be relatively weak in perfect diamond; evidently, little attention was paid to the pioneering work done in England and already alluded to in the Introduction.[2,3] It is now clear that all diamonds are practically opaque ($\beta > 1$ cm^{-1}) in the 2.5- to 7.5- μm wavelength range, but high-quality crystals should exhibit excellent transparency ($\beta < 1 \times 10^{-2}$ cm^{-1}) at wavelengths shorter than 2.5 μm and may have acceptable absorption coefficients ($\beta \simeq 0.1$ cm^{-1}) in the LWIR.

Figure 2 displays the IR absorption spectrum of a polycrystalline diamond specimen produced at Raytheon by means of the microwave-plasma-assisted CVD process: this spectrum reflects the "absorbance" defined as

$$A \equiv \ln(T_O/T), \qquad (2)$$

where T is the measured transmittance and T_O refers to a baseline fit that serves the purpose of eliminating low-frequency contributions originating from both, the surface roughness and the internal scatter. The spectral range (2.5 to 20 μm) is almost the same as the one covered by Thomas and Joseph[18] in their recent investigation of multi-phonon absorption in type-IIa diamond, and the reader will easily convince himself (compare with Fig. 2 of Ref. 18) that, if one disregards the C-H stretch bands at approximately 2900 cm^{-1}, there are no basic differences in terms of spectral features between natural single crystals and state-of-the-art CVD diamonds. The main features are of an intrinsic nature, which gives rise to three distinct regimes as outlined below.

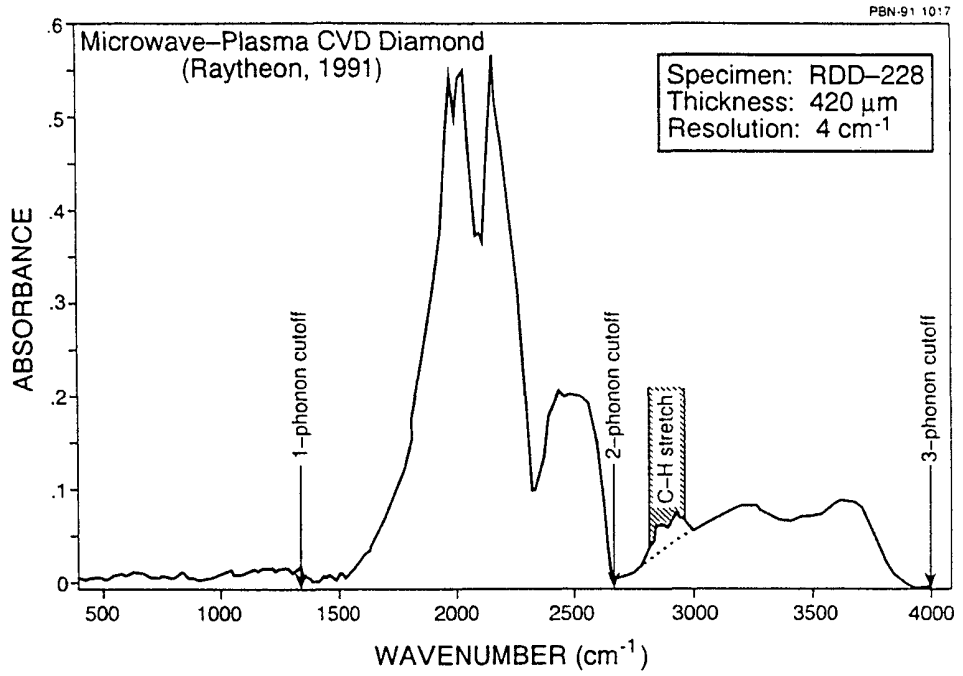

Fig. 2. Infrared absorption spectrum of state-of-the-art CVD diamond (Ref. 21).

(a) The most obvious lesson of Fig. 2 is that the IR absorption occurs primarily in the two- and the three-phonon spectral regions, in other words, in a wavenumber range extending from one to three times the Raman frequency (1333 to 3999 cm^{-1}). The measured absorbance* peaks at frequencies where second-order processes dominate and points to lattice absorption coefficients of *ca.* 12 cm^{-1} at wavelengths of about 5 µm.[2] The C-H stretch bands that enhance the absorption in the three-phonon region (see Fig. 2) appear to be strongly dependent upon the methane pressure in the growth chamber[19] and may prove to be difficult to remove in CVD material.

---

* Note that an absorbance as defined in Eq. (2) yields the correct absorption coefficient ($\beta = A/L$) only if the condition $A << 1$ holds: in Fig. 2, the scale was adjusted on the basis of postulating that, in the two-phonon region, the absorption of CVD diamond should be comparable to that of type-IIa diamond.

(b) At frequencies above 4000 cm^{-1}, that is, in the *n*-phonon region (n>3), the intrinsic absorption of diamond should be very low[20] and stay low throughout the near-IR and the visible up to the electronic edge at *ca.* 0.25 μm. At wavelengths of, say 1 μm, it is reasonable to expect that nearly-perfect single-crystal synthetic diamonds will have absorption coefficients of less than $1\times10^{-4}cm^{-1}$, which suggests applications in the power optics area of potentially major significance. Residual surface impurities, which must be carefully controlled, and/or AR coatings, which will be required in a laser-window environment, then may turn out to be the limiting factors as described in Sec. 4.

(c) In principle, there are no IR-active first-order processes in diamond, but it is known that common imperfections such as impurities, lattice disorder, or even crystalline strain disturb the local symmetry and, thus, may activate single-phonon absorptions.[3] Figure 2, in accord with observations reported in Ref. 18, strongly supports the notion that most, if not all diamonds exhibit a complex pattern of absorption bands at frequencies below the one-phonon cutoff, that is, in a wavelength region (8 to 12 μm) of much current interest. In fact, recent Fourier transform IR spectroscopy performed at Raytheon was quite successful in establishing that the one-phonon absorption features reflect lattice vibrational modes allowed by crystal disorder, in conjunction with impurity-induced "localized" modes primarily due to nitrogen in various states of aggregation; the reader may consult Ref. 21 for more details and an *entrèe* to relevant literature.

2.3. Elastic Anisotropy

In the context of applications such as missile domes or laser windows, an evaluation of the performance of diamond relies on proper values for Young's modulus and Poisson's ratio. Young's modulus of single-crystal diamond is often set equal to $1/s_{11}$, or E=1050 GPa, which assumes[22] that "the modulus does not vary greatly with orientation"; with regard to Poisson's ratio, the data compilation in Field's book[22] lists $\nu\approx0.2$ as an appropriate "average" value. In fact, since the elastic constants of diamond are known with great accuracy (see Table 1), it is a straightforward matter to derive exact numbers for both E and ν, taking into account the anisotropy of the elastic properties as expressed in terms of the anisotropy factor,

$$S = (s_{11}-s_{12}) - s_{44}/2 = 0.180\ TPa^{-1}\ , \quad (3)$$

the constants s_{ij}'s referring to the elastic compliances.

For this purpose, it is recalled that, in a crystallographic plane identified by Miller indices *(hkl)*, Young's modulus and the two Poisson's ratios (ν for in-plane elongations, ν' for out-of-plane elongations) relate to the compliances of cubic material as follows:[23]

$$E_{(hkl)} = (s_{12}+s_{44}/2+S\Omega_{22})^{-1} \quad (4)$$

$$\nu_{(hkl)} = -(s_{12}+S\Omega_{23})E_{(hkl)} \quad (5a)$$

$$\nu'_{(hkl)} = -(s_{12}+S\Omega_{12})E_{(hkl)} \ , \quad (5b)$$

the symbols Ω_{ij} representing functions of the two Eulerian angles in addition to the angle Θ that specifies the direction in the plane.* Hence, it is immediately apparent that planar isotropy requires $S \equiv 0$ unless the functions Ω_{ij}'s reduce to directionally-independent constants. This holds only in the (111) plane, where we have $\Omega_{22}=1/2$, $\Omega_{23}=1/6$, and $\Omega_{12}=1/3$, which leads to $E_{(111)}=1160$ GPa, $\nu_{(111)}=0.0795$, and $\nu'_{(111)}=0.0435$ for single-crystal diamond. Since the morphology of CVD diamond appears to be dominated by (110) planes,[5] it should be of interest to consider the elastic anisotropy in the light of relevant expressions for the Ω_{ij}'s.[23]

$$\Omega_{22} = 9/16 + 1/4\cos(2\Theta) + 3/16\cos(4\Theta) \quad (6a)$$

$$\Omega_{23} = 3/16[1-\cos(4\Theta)] \quad (6b)$$

$$\Omega_{12} = 1/4[1-\cos(2\Theta)] \ , \quad (6c)$$

and to plot both $E_{(110)}$ and $\nu_{(110)}$ as a function of the angle Θ (see Fig. 3). Considering the four-fold symmetry, this polar plot ($0 \leq \Theta \leq \pi/2$) specifies how the elastic properties vary depending upon the direction in the (110) plane and emphasizes the surprisingly large anisotropy of Poisson's ratio in diamond. For highly-textured (110) polycrystalline deposits, I conclude that the appropriate numbers are $\bar{E}_{(110)}=1150$ GPa and $\bar{\nu}_{(110)}=0.0770$, based on a simple averaging procedure.

---

* The direction $\Theta=0$ refers to a principal crystallographic axis.

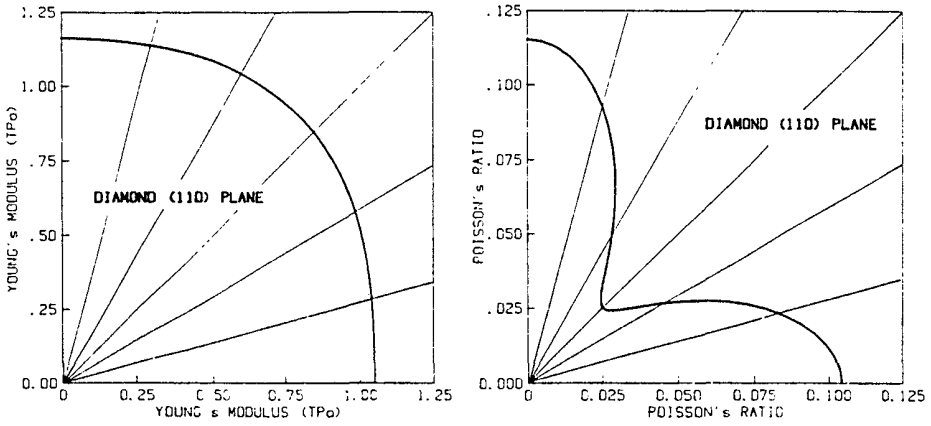

Fig. 3. Young's modulus and Poisson's ratio in the (110) plane of single-crystal diamond.

For the sake of completeness, we may also consider the case of a randomly-orientated aggregate of diamond crystallites and make use of the procedure outlined in Ref. 24 for obtaining the relevant E and ν values. The two Hashin - Shtrikman averages yield almost identical results, $\overline{E}=1140$ GPa and $\overline{\nu}=0.0694$, which are quite consistent with numbers that apply to (110) as well (111) planes and, thus, quite gratifying considering the very nature of the analytical techniques involved; these are the values I recommend in the absence of specific indications regarding the morphological characteristics of a CVD-diamond artifact. In this connection, I may add that recent measurements of the biaxial modulus, $M=E/(1-\nu)$, of hot-filament CVD-diamond films (see Appendix A of Ref. 7) point to $M=(1197\pm98)$ GPa, which demonstrates that state-of-the-art deposits exhibit elastic properties that are fully compatible with the compliances (or stiffnesses) of natural single crystals.

3. HIGH-SPEED MISSILE DOMES

The flight profiles of advanced air-intercept missiles are predicated on significant enhancements in launch velocity, acceleration, and total range. These requirements are driving the present, intense search for "new" IR-transparent materials able to cope with the concomittant erosion problem, the thermally-induced shock, and the dome self-emission.[8] Diamond offers the greatest resistance to rain and dust ero-

sion of any known material, but surface oxidation and bulk graphitization may become limiting factors considering the heat-load conditions encountered at the flight boundary; this situation will be examined in Sec. 3.2. First (Sec. 3.1), I will specify altitudes and velocities typical of projected air-to-air scenarios and present simple formulas for obtaining the required wall thickness of domes that must withstand the pressure differentials arising on a "worst" flight trajectory. This will be done in the context of first-order approximations that emphasize the basic concepts rather than relying on numerical finite-element techniques. The same comment applies to the analysis of dome heating (Sec. 3.2), which involves two distinct parts: (a) An evaluation of stagnation-point temperatures encountered in sustained high-velocity flight including their impact on diamond material in the light of relevant time constants, and (b) An assessment of the thermal shock situation during the transient heating phase, as large temperature gradients develop across the dome wall. In addition, it is essential to verify that thermal radiation originating from the hot dome does not blind the sensor system, in the sense that the background photons do not degrade the signal-to-noise ratio beyond acceptable limits (Sec. 3.3); in effect, this requirement amounts to setting tolerable upper limits for the emittance and, by the same token, for the absorption coefficient of a diamond dome, in the wavelength region of operational interest. *Pour fixer les idées*, I propose to consider the dome configuration shown in Fig. 4: The diameter (2R) is set equal to 10 cm and the acceptance angle (2α) equal to 60 deg, in accord with tentative dome designs considered in Ref. 25. This configuration provides an aperture, $D=2R\sin(\alpha)$, of 5 cm thus minimizing the aerodynamic drag while achieving the desired angular resolution of 0.25 mrad under near-diffraction-limited conditions,

$$\delta = 1.22(\lambda/D) \ , \qquad (7)$$

for IR-imaging seekers operating in the 8- to 12- μm spectral band.

3.1. Dome Thickness

The flight regimes of future air-to-air missiles are expected to cover a wide range of altitudes and speeds, as specified in Table 2 (lines 1 to 3), which summarize U. S. Air Force requirements.[26] The three scenarios refer to "low", "medium", and "high" altitudes of operation thus generating a very broad spectrum of aerostructural/aerothermal loads that must be negotiated by an IR dome

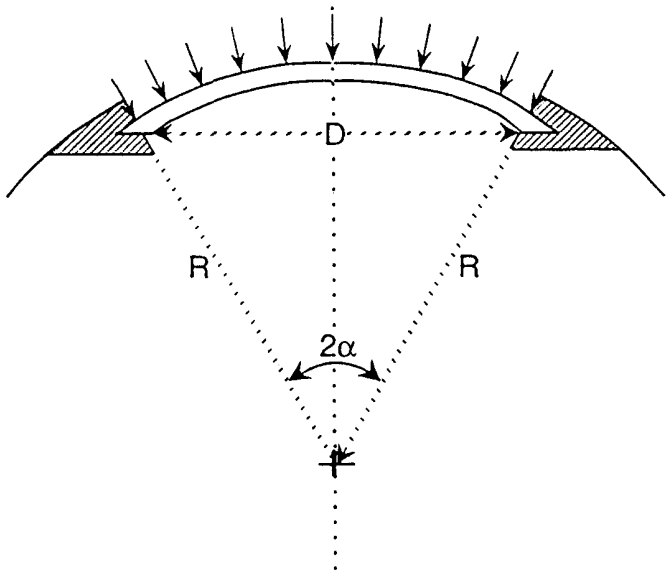

Fig. 4. Proposed diamond dome configuration (R=5cm, α=30 deg).

located in the missile nose section. The thickness of this dome plays a critical role in the sense that it has a major effect on the aerodynamic heating process as well as the infrared self-emission and must, therefore, be given proper attention.

At Mach numbers $M_\infty \geq 3$, the pressure distribution on a spherical shell varies essentially as $\cos^2(\theta)$,[27] which implies that, for truncated hemispheres ($\theta \leq 30$ deg), we may assume that the aerodynamic pressure is uniform and equal to the stagnation-point pressure p_{st}. In highly supersonic flight, a fully-vented IR dome as in Fig. 4 must, therefore, withstand a pressure differential

$$\Delta p = p_{st} - p_\infty = p_\infty [(p_{st}/p_\infty) - 1] \qquad (8)$$

p_{st}/p_∞ referring to the pressure ratio across a normal shock along the stagnation streamline.

$$\frac{p_{st}}{p_\infty} = \frac{[(\gamma+1)M_\infty^2/2]^{\gamma/(\gamma-1)}}{[2\gamma M_\infty^2/(\gamma+1) - (\gamma-1)/(\gamma+1)]^{1/(\gamma-1)}} \cdot \qquad (9)$$

With γ set equal to 1.4 and free-stream pressures p_∞ that are representative of a U. S. Standard Atmosphere, the pressure differentials of interest are as listed on line 6 of Table 2, which reveals

that the medium-altitude scenario produces the most severe pressure load with Δp's as high as 200 psi.

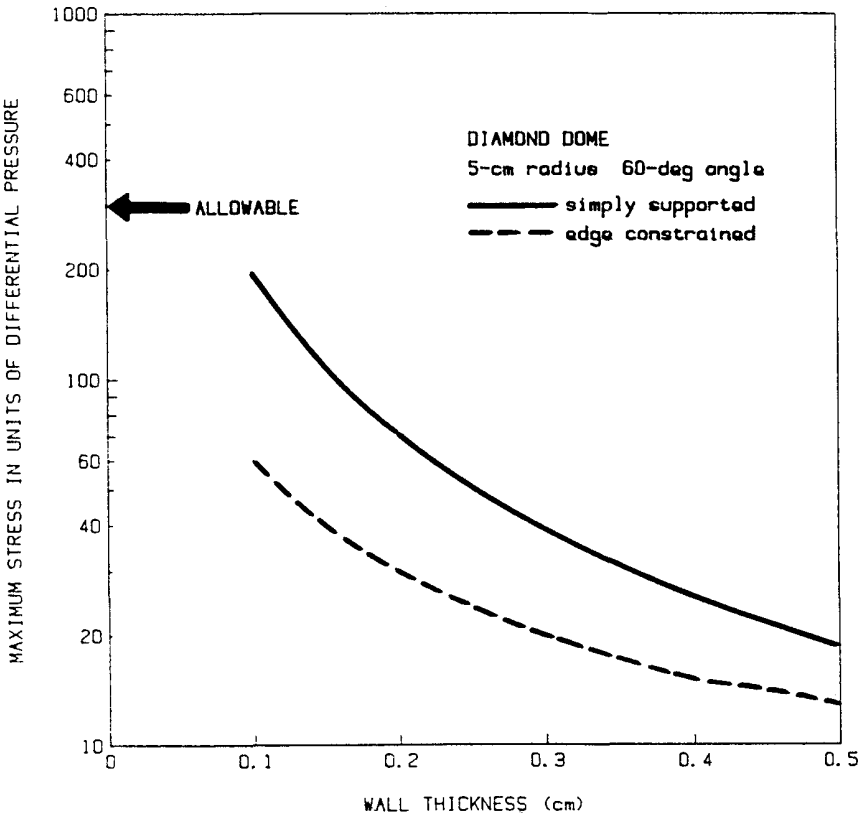

Fig. 5. Calculated peak stress for a diamond dome, under conditions as specified; the allowable stress was set equal to 100 kpsi.

Such pressures give rise to a complex stress pattern that reflects the nature of the edge attachment; for our purposes, it should be sufficient to consider the two limiting cases of (a) the simply-supported shell that bends when submitted to the action of a uniform normal pressure, and (b) the shell with built-in (or clamped) edges that is restrained from moving in the "horizontal" plane. For case (a), the greatest stress is tensile and can be approximated as follows[28]:

$$\frac{\sigma_{max}}{\Delta p} = \frac{R}{2L}\left\{[1.6+2.44\sqrt{\frac{R}{L}}\sin(\alpha)]\cos(\alpha)-1\right\} \qquad (10)$$

if the wall thickness L satisfies the inequalities

$$\frac{R\sin^2(\alpha)}{12} \leq L \leq \frac{R\sin^2(\alpha)}{1.2} \quad . \tag{11}$$

Under similar conditions, any edge-constrained shell experiences a peak stress that is compressive and can be described by a very simple formula.

$$\frac{\sigma_{max}}{\Delta p} = -1.2\frac{R}{L} \quad , \tag{12}$$

where R represents the dome radius. If R=5 cm and α=30 deg as postulated earlier, the two formulas [Eq. (10) and Eq. (12)] hold for wall thicknesses of 1 to 10 mm and yield the $|\sigma_{max}/\Delta p|$ ratios plotted in Fig. 5; as expected, it is the simply-supported shell that exhibits the worst stress. Assuming now that a tensile strength of 400 kpsi (see Table 1) is indicative of the flexural strength of a diamond dome, it follows that the allowable $\sigma_{max}/\Delta p$ ratio must obey the relation

$$\left.\frac{\sigma_{max}}{\Delta p}\right|_{allow} \leq \frac{\sigma_f/SF}{(\Delta p)_{max}} \quad , \tag{13}$$

which implies that the ratio should not exceed, say five hundred considering that pressure differentials of 200 psi are likely to occur and that the safety factor must be set equal to four. Returning now to Fig. 5, it is immediately seen that a 1-mm thick diamond dome mounted on a 5-cm diameter IR aperture will be able to withstand the anticipated pressure loadings.

3.2. Dome Heating

In flight, a missile dome is subjected to aerodynamic heating as a result of the convective heat-transfer process described by the equation

$$q = h(T_r - T_{ow}) \quad , \tag{14}$$

where h represents the heat-transfer coefficient, T_r is the recovery temperature, and T_{ow} refers to the outer wall temperature.* Under

---

* Radiant heat losses, which play a minor role for altitude/speed regimes of interest here, will be disregarded.

laminar flow conditions, as expected for truncated hemispherical domes, the recovery temperature cannot exceed the stagnation temperature.

$$T_{st} = T_{\infty}\left[1+(\gamma-1)M_{\infty}^2/2\right] , \qquad (15)$$

which implies that, in a steady-state situation with no conductive heat losses, a missile dome may reach but cannot exceed temperatures as given by Eq. (15). At supersonic speeds, these temperatures are quite high (see Table 2), which raises the issue of the suitability of diamond as an IR-transmissive material in a high-temperature environment; but first, it must be established that the time frames are such that the surface temperatures can approach stagnation-type limits. For that purpose, we may consider the dimensionless Biot number,

$$Bi \equiv hL/k , \qquad (16)$$

which characterizes the transfer of heat across the boundary layer in relation to the dome's ability to transport the heat. At the stagnation point, the heat-transfer coefficient can be estimated by means of a semi-empirical formula,[29]

$$h_{st}\sqrt{2R} \simeq 1.7c_p\sqrt{\rho_{\infty}\mu_{\infty}a_{\infty}}M_{\infty}(1+0.2M_{\infty}^2)^{0.1} , \qquad (17)$$

which yields numbers as listed in Table 2 and demonstrates that the most-severe thermal environment in terms of temperatures does not correlate with the highest thermal-flux situation. For 1-mm thick diamond domes, such heat-transfer coefficients result in very small Biot numbers (diamond domes are thermally thin!), which in turn suggests thermal time constants[29]

$$t_{th} = \rho C_p L/h_{st} \qquad (18)$$

of the order of 1 sec but at very high altitudes; we conclude that, for flight times of 80 sec or more as contemplated in Ref. 26, diamond missile domes will indeed reach the recovery temperature.

In air, the oxidation rate of diamond becomes relatively significant at temperatures above 600°C (900 K); this is a fact[30] that must be taken into consideration in any assessment of diamond as a sensor window. A diamond dome can readily handle Mach-3 fly-outs at low altitude (see Table 2), but the medium-altitude scenario may well be ruled out unless durable coatings can be found that provide protection against oxygen attack. At very high altitudes, and Mach-6 velocities,

the stagnation temperatures (1860 K) are such that diamond may convert to graphite,[14] which creates more problems that have not yet been properly addressed; fortunately, the large bandgap will preclude a significant electronic population thus ensuring that the IR transmission will not be degraded by free-electron absorption.

Table 2. Key numbers for assessing the performance of diamond missile domes

	SCENARIO	LOW[a]	MEDIUM[a]	HIGH[a]
1.	Flight altitude (km)	1	3	30
2.	Mach number at launch	1	1.5	2
3.	Mach number at speed	3	4	6
4.	Free-stream pressure (psi)	13.0	10.2	0.174
5.	Stagnation pressure ratio	12.0	20.9	46.5
6.	Pressure differential (psi)	143	203	7.91
7.	Free-stream temperature (K)	282	267	227
8.	Stagnation temperature (K)	790	1121	1861
9.	Inner wall temperature (K)	338	387	409
10.	Heat-transfer coeff. ($Wcm^{-2}K^{-1}$)	0.145[b]	0.185[b]	0.036[b]
11.	Biot number	2.2×10^{-3}[c]	2.81×10^{-3}[c]	5.47×10^{-4}
12.	Thermal time constant (sec)	1.23[c]	0.97[c]	4.97[c]
13.	Peak temperature gradient (Kcm^{-1})	9.94[c]	20.6[c]	7.94[c]
14.	Peak thermal stress (psi)	88.7[c]	184[c]	70.8[c]
15.	Thermal shock resistance (dB)	30.5[c]	27.4[c]	31.5[c]

(a) Assumes a Standard Atmosphere and properties as in Table 1.
(b) 10-cm diameter dome.
(c) 10-cm diameter/1-mm thick dome.

For most IR-transmitting materials, the primary cause of failure in a missile-dome application can be attributed to brittle fracture caused by thermal shock; the fracture is induced by tensile stresses on the "cold" side, *i.e.*, the inner surface of the dome. These stresses originate from the sudden temperature gradients generated by aerodynamic heating, which, in conjunction with the thermal expansion, produce compressions on the outer surface and tensions on the inside. As mentioned earlier, it is not the object of this paper to present a complete picture of the

thermal shock phenomenology for diamond sensor windows but, rather, to make correct assessments that may guide us in delineating the key parameters that control the performance. In that context, I rely on the well-known[31] expression for the maximum stress experienced by a clamped plate, or a complete sphere,[28] if there is a linear temperature variation across the thickness and if both are free to expand:

$$|\sigma_{max}| = \frac{\alpha E}{2(1-\nu)} \Delta T \ , \qquad (19)$$

where ΔT refers to the temperature difference between the outer and the inner surfaces,

$$\Delta T = |T_{ow} - T_{iw}| \ . \qquad (20)$$

In a transient situation, ΔT is a strong function of time and depends critically upon the heat-transport process as characterized by the Biot number; specifically, if the condition $Bi < 1$ applies, ΔT peaks when the backface temperature starts to rise, which occurs long before the front reaches the stagnation temperature and, thus, leads to[25]

$$\Delta T_p = (T_{st} - T_{iw})(Bi)_{st} \ . \qquad (21)$$

In a first approximation, therefore, a thermally-thin dome will be subjected to a peak stress that amounts to

$$|\sigma_{max}|_p \simeq \frac{\alpha E}{2(1-\nu)} (Bi)_{st} (T_{st} - T_{iw}) \ , \qquad (22)$$

where $(Bi)_{st}$ refers to the Biot number at the stagnation point, T_{st} is the relevant stagnation temperature, and T_{iw} must be set equal to the wall temperature at the onset of the shock. Assessing the thermal shock resistance (TSR) then boils down to comparing $|\sigma_{max}|_p$ with the allowable stress, $\sigma_f/4$, which is best done by defining TSR as follows:

$$TSR \equiv 10 \times \log \left[\frac{\sigma_f/4}{|\sigma_{max}|_p} \right] \qquad (23)$$

if the results are to be quantified. In this connection [see Eqs. (16) and (22)], we note that the stress ratio can be expressed as a product of three terms,

$$\left|\frac{\sigma_f/4}{\sigma_{max}}\right|_p = \frac{\sigma_f(1-\nu)k}{\alpha E}\cdot\frac{1}{h_{st}L}\cdot\frac{1/2}{T_{st}-T_{iw}} \quad , \qquad (24)$$

the first term involving intrinsic material properties only, the second term depending upon both the diameter of the dome (through the heat-transfer coefficient) and its thickness, while the third term reflects the severity of the aerothermal environment.* For diamond, and upon inserting numbers as listed or derived earlier (see Sec. 2), Eq. (23) yields TSR figures of about 30 dB for the three scenarios, which demonstrates, conclusively, the exceptional thermal shock performance of this material in a missile-dome or a sensor-window application.

3.3. Dome Emission

As the IR dome heats up, it will emit gray-body radiation over the entire electromagnetic spectrum, which may adversely impact the operation of the seeker system in a high-speed flight situation. It is generally recognized that "saturation" of the detectors by radiation from aerodynamically heated domes is not a major issue,[32] but the added "background"-induced noise will lower the effective performance of the system in terms of detection range as well as tracking ability.[33] Previous investigations of the "hot-window problem" always focussed on the 3- to 5-μm spectral region: since diamond is not an acceptable dome-material candidate in this wavelength range (see Sec. 2), I take it that the IR seeker of postulated missiles[26] will be operating in the 8- to 12-μm band, which, incidentally, is attracting renewed attention because it will be quite difficult to mask the LWIR signature of future-generation combat aircraft.

---

* For this reason, evidently, the first term is often used as a "figure of merit" for ranking the TSR performance of IR materials (see Sec. 1). This practice must be discontinued on the following grounds: (a) Equation (24) does not apply at all when the Biot number is larger than one, *i.e.*, for thermally-thick domes, and (b) Even if the Bi<1 criterion holds, it should be kept in mind that the thickness L is a function of the fracture strength, which suggests that a figure of merit as given in Eq. (1) does not properly "weigh" the importance of fracture strength in determining the thermal shock resistance.

I am also assuming that (a) the seeker system has a wavelength-independent "optical efficiency," (b) the sensor subsystem is detector-noise limited, and (c) the detector elements all operate in a BLIP mode. The peak-signal to rms-noise ratio at the output terminals of the signal-processing unit then can be expressed as follows[33]:

$$SNR = H_{eff}/NEI \tag{25}$$

if the symbol H_{eff} designates the net effective irradiance originating from the target, while NEI is the noise-equivalent irradiance.

$$NEI = (NEI)_O\sqrt{\Phi/\Phi_O} \ , \tag{26}$$

expressed in terms of the laboratory-measured $(NEI)_O$ and the background photon-flux ratio Φ/Φ_O. The noise voltage is seen to be proportional to the square root of the number of incident background photons, which demonstrates that the signal-to-noise ratio in the presence of hot-irdome radiation can be derived from the "dark-system" SNR simply by writing

$$SNR = \frac{(SNR)_O}{\sqrt{\Phi/\Phi_O}} \ . \tag{27}$$

The ratio Φ/Φ_O thus determines the performance degradation induced by environmental factors and must be evaluated with some care considering that the noise photons originate from three distinct sources: the detector surroundings, the background scene, and the hot dome. If, for the sake of simplicity, we assume that the dome emittance is independent of wavelength and temperature, in the spectral range of interest, the photon-flux ratio can be expressed in a relatively compact manner,[33]

$$\frac{\Phi}{\Phi_O} = \tau_O \frac{(1-\bar{E})Q(T_B)+(1/\tau_O-1)Q(T_S)+\bar{E}Q(T_D)}{Q(T_O)} \ , \tag{28}$$

the symbol Q(T) representing the effective quantum exitance at the temperature T, *i.e.*,

$$Q(T) = \int_{8\ \mu m}^{12\ \mu m} \frac{2\pi c\lambda^{-4} d\lambda}{\exp(c_2/\lambda T)-1} \quad , \tag{29}$$

for the 8- to 12-μm band. Keeping in mind that the optical efficiency, in other words, the transmittance of the optics including obscurations but not the filter, should be of the order of 50% for state-of-the-art IR seekers, it becomes an easy matter to describe the window-induced SNR degradation (in decibels) simply by plotting the function

$$10 \times \log[SNR/(SNR)_o] = -5 \times \log(\Phi/\Phi_o) \tag{30}$$

against the dome temperature, for fixed values of the average emittance $\bar{E}$, as in Fig. 6.

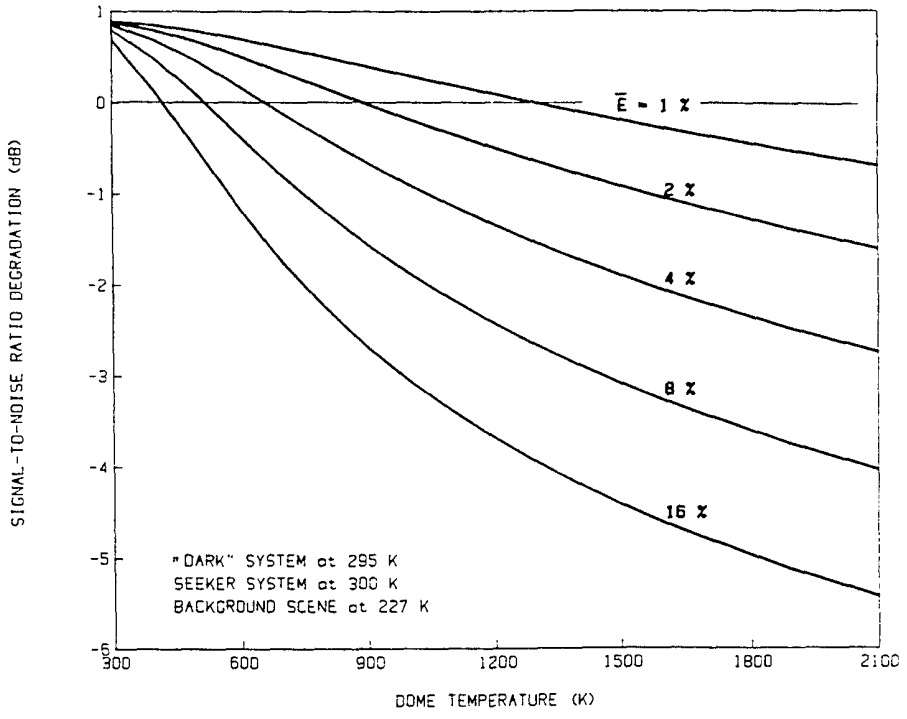

Fig. 6. Signal-to-noise ratio degradation as a function of the dome temperature for fixed values of the average dome emittance: the reference SNR is that of the "dark" system, i.e., as measured in a laboratory setting.

Since the background-scene temperature was set equal to 227 K (high-altitude scenario), the signal-to-noise ratio improves for "cold" domes but, depending upon the emittance, at some point the ratio will drop below the reference value as the dome becomes "hot". For the sake of the argument, I am postulating that, in an operational environment, a degradation of more than 3 dB cannot be tolerated; Figure 6 then suggests that the emittance cannot exceed 15% at 1000 K, or 5% at 2000 K. From the relation

$$\bar{E} \simeq (1+\bar{R})\bar{\beta}L \ , \qquad (31)$$

which holds for an IR dome coated on the inside, it follows that the average absorption coefficient of a 1-mm thick dome, which is expected to function properly at temperatures above 1000 K, should not exceed, say 1 cm^{-1} in the 8- to 12-μm band.* In the light of the discussion presented in Sec. 2.2, this may not be an unrealistic goal for CVD diamond, especially since single-phonon induced absorptions do not exhibit much temperature dependence.[20]

4. HIGH-POWER LASER WINDOWS

The predicted very low absorption at wavelengths near 1 μm combined with an exceptionally high thermal conductivity at temperatures near 77 K (see Sec. 2) makes diamond a "natural" for free-electron-laser (FEL) window applications. Consider a laser cavity with a circular output-aperture window mounted as in Fig. 7: The window is edge-cooled by means of a liquid-nitrogen heat exchanger and is made of defect-free diamond, AR-coated, and preferably (111) orientated. I propose to assess the performance of this configuration by relying upon well-established analytical procedures[34] and to point out potential limitations deriving from the refractive index characteristics of

---

* In the absence of any coating on the outer surface, such a dome transmits about 75% of the incident radiation, which should be quite satisfactory. Note, however, that making the dome thicker for the purpose of augmenting the thermal time constant [see Eq. (18)] carries a penalty in terms of the tolerable absorption coefficient, as evidenced via Eq. (31).

diamond. For that purpose, I will first (Sec. 4.1) describe the temperature profiles generated by incident Gaussian beams since radial temperature gradients create optical distortion and, thus, may inject unacceptable aberrations. This problem will be examined in Sec. 4.2, where I derive formulas for the power-handling capability and the allowable peak intensity under continuous as well as pulsed laser running conditions. In addition (Sec. 4.3), I will demonstrate that maintaining the window at low temperature, in a high-power environment, implies a minimum thickness L that far exceeds pressure-related requirements.

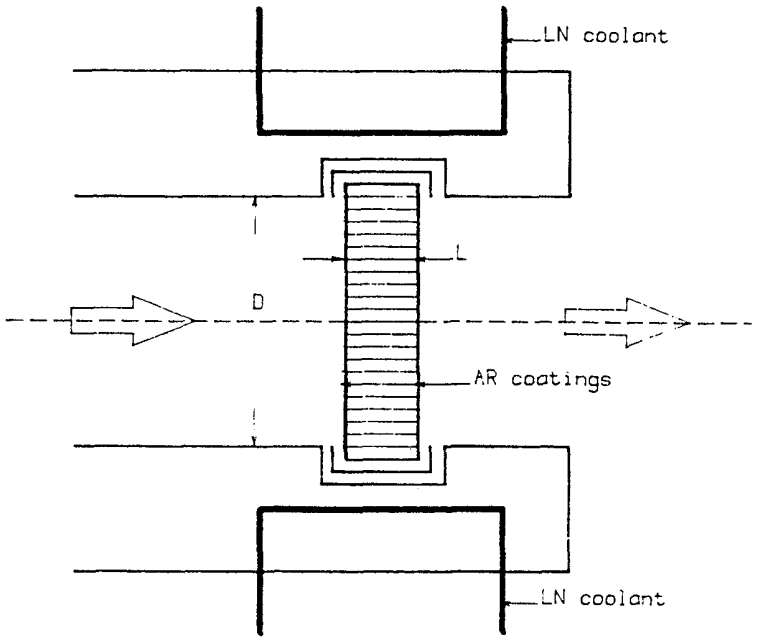

Fig. 7. Schematic of an edge-cooled (liquid nitrogen) cavity laser window.

4.1. Window Temperature Profile

In a cylindrical geometry, Gaussian beams of width w,

$$I(r) = I_o \exp(-2r^2/w^2) \ , \qquad (32)$$

transmitted through an aperture of diameter D are best described in terms of the truncation parameter W,

$$W = \frac{(D/2)^2}{w^2} \quad , \tag{33}$$

if one makes use of the dimensionless variable $\rho = r/(D/2)$ to define the radial position:

$$I(\rho) = I_o \exp(-2W\rho^2) \quad . \tag{34}$$

The power transmitted through the aperture,

$$P = 2\pi \int_o^{D/2} I(r)dr \quad , \tag{35a}$$

may then be expressed in the following manner:

$$P = \frac{\pi(D/2)^2 I_o}{2W} \left[1-\exp(-2W)\right] \quad , \tag{35b}$$

which assigns specific meaning to the parameter W. In effect, for large truncation-parameter values (W>2), Eq. (35b) reduces to

$$P = \frac{\pi(D/2)^2 I_o}{2W} \quad , \tag{36}$$

thus relating the transmitted power to the on-axis intensity in a straightforward manner: I will assume that this relation always holds for laser beams of interest here.

For edge-cooled cylindrical windows, the steady-state heat-flow equation takes the form[34]

$$k\left[\frac{d^2(\delta T)}{dr^2} + \frac{1}{r}\cdot\frac{d(\delta T)}{dr}\right] + \beta I_o \exp(-2r^2/w^2) = 0 \tag{37}$$

if δT represents the beam-induced temperature increase, averaged over the thickness of the window, and β is the effective absorption coefficient of the window medium. In terms of the radial variable ρ, and taking the relation (36) into account, we may rewrite the heat-flow equation as follows:

$$\frac{d^2(\delta T)}{d\rho^2} + \frac{1}{\rho}\cdot\frac{d(\delta T)}{d\rho} + \frac{2W}{\pi}\cdot\frac{\beta P}{k}\exp(-2W\rho^2) = 0 \quad , \tag{38}$$

thus introducing the factor $\beta P/k$, which has the dimension of a temperature. This allows us to further "streamline" the analysis by expressing δT in units of $\beta P/k$, *i.e.*, by setting

$$\delta T(\rho) \equiv (\beta P/k)\,\delta T^{*}(\rho) \ , \tag{39}$$

the star denoting that this is a normalized temperature. The procedure then leads to

$$\frac{d^2(\delta T^{*})}{d\rho^2} + \frac{1}{\rho}\cdot\frac{d(\delta T^{*})}{d\rho} + \frac{2W}{\pi}\exp(-2W\rho^2) = 0 \ , \tag{40}$$

which demonstrates that beam-induced temperature gradients scale with $\beta P/k$, that is, the power deposited per unit path length and the inverse thermal conductivity of the medium. Regarding boundary conditions, it is clear that, because of the azimuthal symmetry, the solution must satisfy the condition

$$d(\delta T^{*})/d\rho\,\big|_{\rho=0} = 0 \tag{41a}$$

on axis; at the edge, we may set the temperature increment equal to zero,

$$\delta T^{*}(\rho)\,\big|_{\rho=1} = 0 \ , \tag{41b}$$

which amounts to using the edge temperature as a baseline.* As shown in appendix B of Ref. 34, the solution of this system [Eqs. (40-41)] can be expressed in closed form:

$$\delta T^{*}(\rho) = \frac{1}{2\pi}\left\{\frac{1}{2}\left[E_1(2W) - E_1(2W\rho^2)\right] - \ln(\rho)\right\} \ , \tag{42}$$

the function $E_1(z)$ denoting an exponential integral.[35]

---

* This is acceptable because thermal lensing is caused by temperature gradients only; these gradients reflect the transport of heat towards the edge but are independent of the actual heat-transfer mechanism to the coolant.

Figure 8 (left-hand side) illustrates the shape of standard Gaussian beams [Eq. (34), the truncation parameter ranging from 1 to 8], which all transmit the same amount of power P, thus emphasizing that large W's signify narrow beams. The temperature profiles they generate in the radial direction of edge-cooled windows are shown on the right-hand side, which illustrates the results of evaluating Eq. (42), thus providing convenient reference numbers for obtaining the true temperature distribution simply through multiplication by βP/k. As anticipated, at fixed beam-power levels, high-truncation-parameter Gaussians generate increasingly steeper temperature profiles, which will be reflected in the magnitude of the thermally induced aberration.

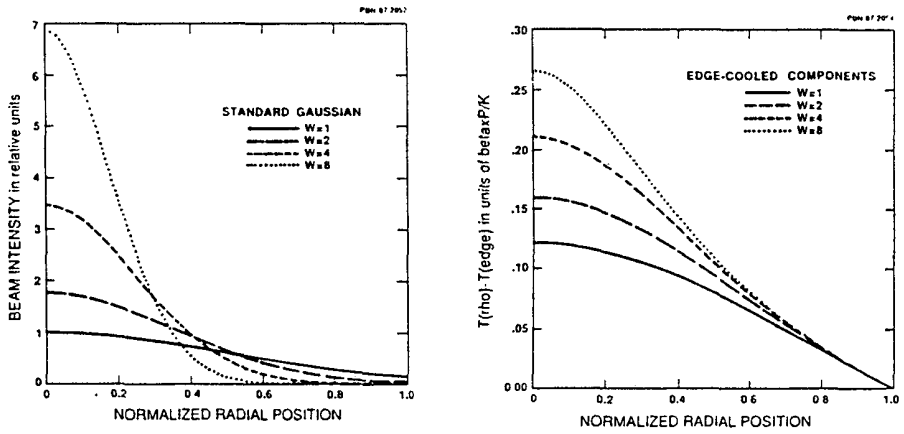

Fig. 8. Beam profile of incident Gaussians and radial temperature distribution of edge-cooled windows, the truncation parameter ranging from 1 to 8; the total transmitted power is kept constant.

4.2. Power-Handling Capability

For IR transmitting materials such as diamond, which have positive thermo-optic coefficients, the phase-aberration function effectively "maps" the radial temperature profile, *i.e.*,

$$\delta\phi(\rho) = (2\pi/\lambda)L\chi\delta T(\rho) \qquad (43)$$

if χ represents the optical distortion coefficient. This coefficient[36] combines contributions to optical distortion due to the change in index

caused by temperature gradients, the change in optical path length caused by thermal expansion, and the stress-optic effects which may induce some birefringence but do not affect the thermal lensing process if the condition $dn/dT>0$ applies; for diamond, therefore,

$$\chi = dn/dT + (n-1)\alpha(1+\nu) \quad , \tag{44}$$

which, *de facto*, reduces to $\chi \simeq dn/dT$, irrespective of the aspect ratio L/D, considering the extremely small expansion coefficient at low temperatures (see Table 1). Remember now that the beam-induced temperature distribution of edge-cooled components can be approximated by means of a fourth-order even polynomial,

$$\delta T(\rho) \simeq (\beta P/k)\left[\delta T_0^* - \delta T_2^* \rho^2 + \delta T_4^* \rho^4\right] \quad , \tag{45}$$

as shown in Ref. 34. This allows us, through substitution into Eq. (43), to obtain a power-series expansion for the aberration function,

$$\delta\phi(\rho) \simeq \delta\phi_0 - \delta\phi_2 \rho^2 + \delta\phi_4 \rho^4 \quad , \tag{46}$$

which tells us immediately that the quartic term,

$$\delta\phi_4 \rho^4 = (2\pi/\lambda) L\chi(\beta P/k)\delta T_4^* \rho^4 \quad , \tag{47}$$

will be responsible for the beam-induced aberration. Since "failure" through excessive generation of spherical aberration reflects an RMS wavefront deformation that exceeds the $\lambda/14$ limit,[37] in other words, if

$$(\lambda/2\pi)\left[\delta\phi_4 \rho^4\right]_{RMS} > \lambda/14 \tag{48}$$

signifies too much distortion, it follows that near-diffraction-limited operation of the window requires that the condition

$$L\chi(\beta P/k)\delta T_4^* \left[\rho^4\right]_{RMS} \leq \lambda/14 \tag{49}$$

must be satisfied. Introducing now the concept of a spherical aberration factor,[34]

$$S^* = \delta T_4^* \sqrt{<\rho^8> - <\rho^4>^2} \quad , \tag{50}$$

where the brackets refer to beam-amplitude weighted averages over the entire aperture, the condition (49) reduces to

$$L\chi(\beta P/k)S^{*} \leq \lambda/14 \ , \tag{51}$$

which is very convenient for our purposes since the factor S^{*} involves only the truncation parameter W.

The central result of this analysis can now be formulated in a concise manner: The power P_l that passes through the window without generating excessive distortion (the allowable beam power level) is given by the formula

$$P_l = \frac{(\lambda/14)k}{\beta L\chi S^{*}} \tag{52}$$

and, therefore, is essentially independent of the aperture/window diameter as well as the heat-transfer coefficient.* Furthermore, since AR coatings are required to avoid potentially catastrophic reflections, the absorptance of the window, $\beta L = 2\beta_S + \beta_V L$, may well be dominated by surface-absorption losses, which implies that, with diamond, the allowable beam power should also be independent of the window thickness. The pertinent numbers I made use of in evaluating P_l are listed in Tables 1 and 3; they yield $P_l \approx 750$ kW at a wavelength of 1 μm, which is quite impressive and far exceeds the power-handling capability of presently available laser-window materials[38] but falls short of the "tens to hundreds of megawatts" predicted by Singer.[9] Three comments are in order: (a) The spherical aberration factor for edge-cooled windows covers the range 0.015 to 0.035 depending on the parameter W;[34] I selected a value of 0.0165, which corresponds to W=10, because the "pencil beams" of projected high-power FELs will be very narrow, perhaps no more than 1-mm wide.[9] (b) Based on presently available dn/dT data,[13] the optical distortion coefficient of diamond ($\chi \approx 1\times10^{-5}K^{-1}$) appears to be reasonably attractive but does not compare with the distortion coefficient of a window-material candidate such as CaF_2.

---

* The aperture enters the formula through the truncation parameter and may impact the aberration factor S^{*}: the heat-transfer coefficient controls the temperature rise at the edge (see Sec. 4.3) and may affect the performance through the temperature dependence of the thermal conductivity k.

which is at least an order of magnitude smaller.[36] (c) It is the thermal conductivity that gives diamond its major advantage; if cooling is required, this means that steps must be taken to prevent excessive beam-induced heating (see Sec. 4.3).

Table 3. Free-electron laser characteristics and relevant diamond-window properties

Laser Wavelength:	λ	=	1 μm	Postulated
RF Power Frequency:	f	=	500 MHz	Ref. 9
Micropulse Duration:	τ	=	50 psec	Ref. 9
Pulse Spacing:	N	=	10	Ref. 9
Truncation Parameter:	W	=	10	Postulated
Aberration Factor:	S^*	=	0.0165	Ref. 34
Bulk Absorption Coefficient:	β_v	<	$1\times10^{-4}cm^{-1}$	Postulated
AR Coating Absorption:	β_s	=	1×10^{-3}	Ref. 38
Optical Distortion Coeff.:	χ	=	$1\times10^{-5}K^{-1}$	This work(a)
Young's Modulus:	E	=	1160 GPa	(111)stress(b)
Poisson's Ratio:	ν'	=	0.0435	(111)stress(b)
Thermal Diffusivity:	κ	=	1720 cm^2sec^{-1}	At 77 K(c)

(a) Assumes a thermo-optic coefficient as in Table 1.
(b) Based on compliances as in Table 1.
(c) For k, ρ, and C_p as in Table 1.

In a CW mode of operation, the allowable beam intensity on axis derives immediately from the allowable power level [see Eq.(36)]:

$$(I_0)_1 = \frac{2WP_1}{\pi(D/2)^2}, \tag{53}$$

which yields almost 20 MW/cm^2 for a 1-cm diameter aperture if P_1 and W are as stated earlier. Consider now the "micropulse" operational regime of RF/FEL's as described in Ref. 9: The allowable peak intensity, $(I_p)_1$, can be much larger since $(I_p)_1$ relates to the average allowable intensity, $(\bar{I})_1$, by way of the duty factor.

$$(I_p)_1 = (\bar{I})_1/DF \ , \qquad (54)$$

which reflects the frequency of the RF source, the pulse duration, and the pulse spacing (DF=fτ/N). For typical values as listed in Table 3, and on assuming that 20 MW/cm^2 is an applicable number for the average intensity, we find that, in principle, peak intensities of 8 GW/cm^2 could be passed without degrading the beam quality; this conclusion, however, disregards observations[39] regarding non-linear processes (two-photon absorption) in diamond, which point to self-focussing effects at the gigawatt-per-square-centimeter intensity level.

4.3. Window Thickness Requirements

Under high-average-power loading conditions, other failure modes besides thermal lensing may enter into play: Beam-induced temperature increments and beam-induced thermal stresses can be limiting factors and must be properly assessed. For edge-cooled laser windows, the temperature increase originates not only from the radial distributions illustrated in Fig. 8 but also from the temperature discontinuity at the edge that develops because of the finite heat-transfer coefficient:

$$\Delta T(\rho) = \frac{\beta P}{k}\delta T^*(\rho) + \frac{\beta P}{\gamma \pi D h_E} \qquad (55a)$$

$$\Delta T(\rho) = \frac{\beta P}{k}\left[\delta T^*(\rho) + \frac{1}{(Bi)_X}\right] \qquad (55b)$$

if $(Bi)_X$ represents the Biot number of the heat exchanger. Assume now that the Biot number can be made much larger than unity by augmenting the contact area through proper design of the window mounting fixture (see Fig. 7) and by using layered films at the edge interface to provide "acoustic matching" as discussed in Ref. 3. The temperature excursion on axis, averaged over the thickness, then amounts to

$$\Delta T_0 \simeq \frac{\beta P_1 \delta T_0^*}{k} = \frac{(\lambda/14)\delta T_0^*}{L\chi S^*} \qquad (56)$$

at the allowable beam-power level [see Eq. (52)]. This temperature increment ΔT_0 should not exceed a certain limit, primarily because the thermal conductivity of high-quality diamond falls off significantly at temperatures much above 77 K, which may degrade the optical power-handling capability. This requirement immediately translates into a minimum thickness criterion for diamond laser windows: Since the ratio $\delta T_0^*/S^*$ is a function of the truncation parameter only and can be approximated by means of a quadratic polynomial, Eq. (56) leads to

$$L \geq \frac{\lambda/14}{(\Delta T_0)_1 \chi}(6.406-0.856W+0.194W^2) \quad , \tag{57}$$

which suggests a minimum thickness of, say 2.5 mm to prevent temperature excursions of no more than 50 K (averaged over the thickness), if $\lambda=1$ μm and $W=10$.

At this point, we may recall that laser windows must have pane-thickness to pane-diameter ratios that satisfy the two following conditions[40]:

$$\frac{L}{D} \geq 0.554\left[\frac{\Delta p}{\sigma_f/SF}\right]^{1/2} \tag{58a}$$

and

$$\frac{L}{D} \geq 1.01\left[(n-1)\left(\frac{\Delta p}{E}\right)^2\left(\frac{D}{\lambda}\right)\right]^{1/5} \quad . \tag{58b}$$

Equation (58a) derives from the requirement that the thickness must be sufficient to prevent fracture under pressure loadings, whereas (58b) takes care of the need to avoid excessive pressure-induced optical distortions. The superior strength of diamond, in conjunction with the enormous modulus, both imply very small aspect ratios ($L/D \approx 0.01$) thus permitting the use of very thin windows in a low-power laser device; as demonstrated above, this does not apply in a high-photon-flux environment because of the requirement to dissipate the heat deposited in the coatings.

Finally, it should be of interest to briefly consider the thermal stress situation in diamond windows that operate at high-average-power levels for the reason that, with presently available laser-window materials, these stresses represent the primary failure mechanism.[38]

Averaged over the thickness, the planar stresses relate to the temperature distribution as follows.*

$$\sigma_\rho(\rho) = \frac{\alpha E \beta P}{k}\left[\frac{\delta T_2^*}{4}(\rho^2-1) + \frac{\delta T_4^*}{6}(1-\rho^4)\right] \qquad (59a)$$

$$\sigma_\theta(\rho) = \frac{\alpha E \beta P}{k}\left[\frac{\delta T_2^*}{4}(3\rho^2-1) + \frac{\delta T_4^*}{6}(1-5\rho^4)\right], \qquad (59b)$$

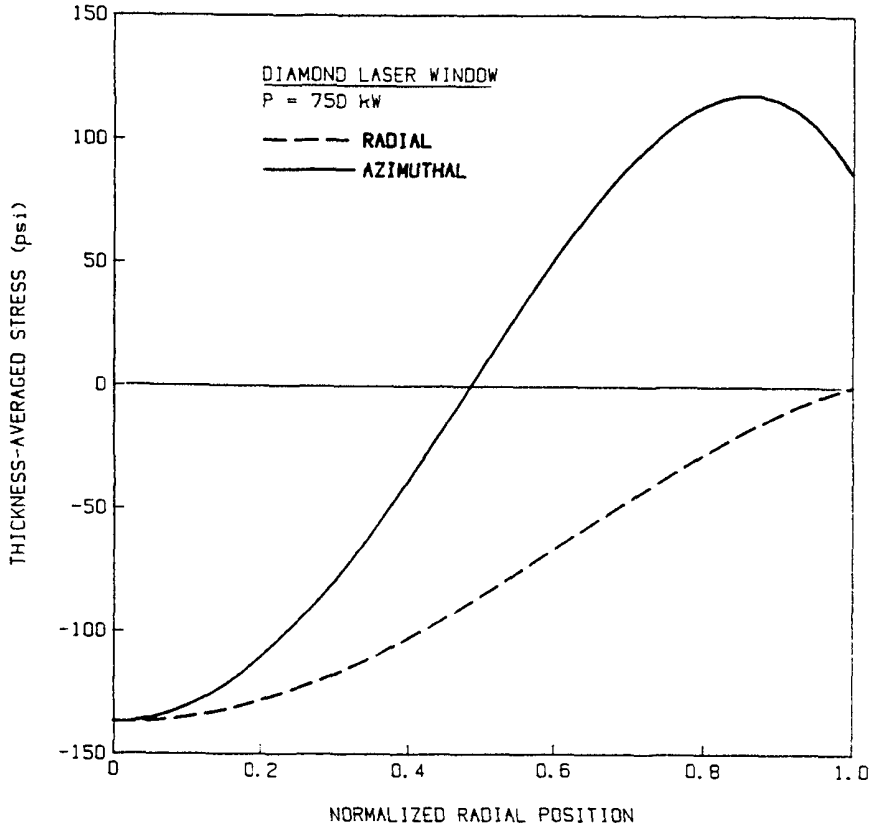

Fig. 9. Radial and azimuthal stresses in a diamond laser window subjected to a 750-kW CW Gaussian beam; the truncation parameter was set equal to ten.

* In principle, the radial temperature distribution produces planar stresses as predicted by thin-plate theory (see Ref. 31), but axial temperature gradients induced by the coatings may lead to a "redistribution" of the state of stress, which is not fully understood.

for steady-state profiles described by Eq. (45); this holds for laser run times larger than the characteristic time for thermal diffusion,

$$t_c = D^2/(\pi^2 \kappa) \quad , \qquad (60)$$

which amounts to about 60 μsec for a 1-cm diameter diamond window. As shown in Fig. 9, the tensile hoop stress barely exceeds 100 psi at the allowable power level, which again confirms that diamond windows exhibit exceptional tolerance to thermal loads, evidently [see Eq. (59)] as a result of the unusually favorable combination of high thermal conductivity and low thermal expansion, particularly at liquid nitrogen temperatures.

5. CONCLUSION

There are very few IR-transmitting materials with mechanical and thermal properties that make them suitable for highly demanding tasks such as airborne FLIRs, missile domes, or laser windows. Currently, the search for "new and improved" infrared materials appears to be motivated by the need to obtain durable, high-speed missile domes for the 3- to 5- as well as the 8- to 12-μm bands, and diamond has always been attracting attention in that context.[25] Recent success in producing large, free-standing deposits of cubic carbon has stimulated substantial efforts in this direction since the properties of the deposits match those of natural diamond: it has also given rise to much speculation about CVD diamond as an "ideal" optical material for a wide range of engineering uses, which is a fallacy (or a fiction)...

(a) Monolithic diamond deposits lack the degree of transparency required for operation as transmissive optics elements in the mid-IR (see Sec. 2.2). At longer wavelengths, it can be reasonably expected that single-phonon absorptions induced by lattice defects and residual impurities[21] will be tolerable in the sense that self-emission phonomena at elevated temperatures should not be "catastrophic," but little data presently exist to confirm this. The difficulty relates to optical scatter arising from the polycrystalline morphology and the surface roughness of CVD deposits: practical solutions depend on new methods of surface polishing to overcome the intrinsic hardness of diamond, and/or modified deposition methods to produce smoother surfaces.

(b) The features that confer diamond it's main advantage under thermally severe loads are the thermal conductivity, which is much larger, and the thermal expansion, which is much smaller than those of other window/dome material candidates. A good thermal conductivity implies small temperature gradients, and small temperature gradient simply a good thermal shock resistance [Eq. (23)] if the "figure of merit" $\sigma_f(1-\nu)/(\alpha E)$ is adequate. Analytical modeling as carried out in Secs. 3.2 and 4.3 suggests that diamond has orders of magnitude more TSR than some of the best competing materials, *i.e.*, the metal oxides which may fail as a result of fracture caused by thermally induced stresses.[25]

(c) The measured tensile strength (≈3 GPa) of natural[11] as well as synthetic[14] diamond appears to be much lower than anticipated for material of such exceptional stiffness (E≈1100 GPa); this may result from unavoidable imperfections and flaws, but further studies must be carried out to ascertain the ultimate strength of diamond and, also, whether CVD diamond can be fabricated with the desired degree of perfection. Surface hardness, rain-erosion resistance, and chemical inertness are unmatched and, therefore, of enormous interest for near-term applications such as protective coatings on existing IR windows. Oxygen gas, however, will attack diamond at temperatures above 600°C, which can be a serious drawback in the context of some projected flight environments (see Sec. 3.1).

(d) There is little doubt that CVD diamond technology will provide a credible if not outstanding LWIR dome material for tactical missiles operating at speeds up to but not beyond Mach 4 in the atmosphere. Since AR coatings are probably ruled out, the transmittance of such domes will be determined by Fresnel reflections, which some workers[26] consider to be a handicap because the refractive index of diamond is rather high (n≈2.38). It should be remembered, however, that the "hot-window problem," *i.e.*, the self-emission of the dome, represents a more serious threat in terms of the signal-to-noise ratio of the seeker system; as demonstrated in Sec. 3.3, this is the element that controls the optical performance of diamond missile domes at high speeds, and present indications[19] lead us to believe that CVD diamond will in fact be sufficiently transparent in the 8- to 12-μm spectral band, especially since small-aperture diamond domes can be made very thin.

(e) For large sensor-window applications, the usefulness of conventional LWIR materials such as ZnS is basically limited by poor mechanical properties, which translates into poor rain-erosion resistance. Since monolithic diamond windows may not soon become available in the sizes required for advanced aerospace missions, the option of depositing CVD diamond protective layers has been frequently mentioned in the literature.[4] Some of the relevant issues have been examined elsewhere (see Sec. 1); the reader should also keep in mind that exoatmospheric flight regimes may involve temperatures that approach the graphitization limit, which, unfortunately, calls for "face-cooling" type solutions with all their attendant difficulties.

(f) Impurity-free, single-crystal diamond, preferably (111) orientated to avoid anisotropic elastic responses, should be a very valuable candidate for high-average-power laser window applications in the near-IR. As discussed in Sec. 4, the power-handling capability will be limited by thermal lensing, which can only be eliminated if absorption-free AR coatings become available; another limitation concerns the edge heat-transfer coefficient, which must be way above the state of the art to avoid nullifying the advantage derived from the superior thermal conductivity at low temperatures. For very-high-peak-power operation, as contemplated for RF/FEL defense systems, or required for laser ICF drivers, diamond windows are not particularly promising considering the non-linear index of refraction,[39] which may induce highly damaging self-focussing effects.

6. ACKNOWLEDGMENTS

I am indebted to Dr. C. Willingham, of Raytheon Research Division, for providing Fig. 1 and to Ms. A. Goguen for her assistance in preparing the manuscript. This paper was written at the suggestion of Dr. R. Hartmann, of Martin-Marietta Electronic Systems, and first presented at the SPIE *Critical Review* Conference on Optical Design, which was held in Orlando/FL, 2-3 April 1991. Support was made available by Raytheon Company through its Independent Research and Development Program.

APPENDIX: LIST OF SYMBOLS

a: sound velocity
A: infrared absorbance
Bi: Biot number
c: velocity of light
c_2: second radiation constant
c_p: specific heat of air
C_p: specific heat of diamond
D: aperture diameter
E: Young's modulus
$\bar{E}$: average emittance
h: heat-transfer coefficient
h_E: edge heat-transfer coeff.
H_{eff}: effective target irradiance
I: beam intensity
I_o: beam intensity on axis
$\bar{I}$: average beam intensity
k: thermal conductivity
L: dome/window thickness
M: Mach number
n: index of refraction
p: dynamic/static pressure
P: transmitted beam power
q: heat flux
r: radial position
R: dome radius
$\bar{R}$: average reflectivity
s_{ij}: elastic compliances
$\hat{S}$: anisotropy factor
S^*: spherical aberration factor
t_c: characteristic diffusion time
t_{th}: thermal time constant
T: infrared transmittance
T_{iw}: inner-wall temperature
T_{ow}: outer-wall temperature
T_r: recovery temperature
T_B: background scene temp.
T_D: infrared dome temperature
T_S: seeker-system temperature
w: beam width
W: truncation parameter

α: thermal expansion coefficient
β: absorption coefficient
γ: specific heat ratio (Sec. 3)
γ: geometric enhancement factor
δ: diffraction angle
δT: radial temperature increment
δT_i: polynomial expansion coeff.
$\delta\phi$: phase aberration
$\delta\phi_i$: polynomial expansion coeff.
Δp: pressure differential
ΔT: total temperature increase
ΔT_o: temperature increase on axis
Θ: directional angle
κ: thermal diffusivity
λ: optical wavelength
μ: atmospheric viscosity
ν: Poisson's ratio, in plane
ν': Poisson's ratio, out of plane
ρ: dimensionless radial position
σ_f: fracture strength
σ_Θ: azimuthal stress
σ_ρ: radial stress
τ_o: seeker optical efficiency
χ: optical distortion coefficient
Φ: background photon flux
Ω_{ij}: directionality functions

DF: duty factor
NEI: noise-equivalent irradiance
RMS: root mean square
SF: safety factor
SNR: signal-to-noise ratio
TSR: thermal shock resistance

sub l: allowable value
sub p: peak value
sub st: stagnation-point value
sub o: laboratory-setting value
sub ∞: free-stream value
sup *: normalized value

REFERENCES

1. R. Ditchburn, "Diamond as an optical material for space optics," *Optica Acta*, vol. 29 (1982), pp. 355-9.
2. J. Hardy and S. Smith, "Two-phonon infrared lattice absorption in diamond," *Philosophical Magazine*, vol. 6 (1961), pp. 1163-72.
3. S. Smith and J. Hardy, "Activation of single-phonon IR lattice absorption in neutron-irradiated diamond," *Philosophical Magazine*, vol. 5 (1960), pp. 1311-4.
4. J. Venables, ed., "Status and applications of diamond and diamond-like materials: an emerging technology," *Document no. NMAB-445* (National Academy Press, Washington/DC, 1990).
5. W. Yarbrough and R. Messier, "Current issues and problems in the chemical vapor deposition of diamond," *Science*, vol. 247 (1990), pp. 688-96.
6. P. Klocek, J. Hoggins, P. Taborek, and T. McKenna, "CVD diamond growth by DC plasma torch," *SPIE Proceedings*, vol. 1325 (1990), pp. 63-72.
7. C. Klein, "Thermal stress modeling for diamond-coated optical windows," *Proceedings of the Twenty-Second Annual Symposium on Optical Materials for High-Power Lasers* (SPIE Press, Bellingham/WA, 1991), pp. 488-510.
8. R. Schwartz, "The Navy research program in LWIR dome materials," *Proceedings of the Second DoD Electromagnetic Windows Symposium* (AEDC, Arnold AFS/TN, 1987), vol. 1, pp. 65-73.
9. S. Singer, "Diamond: a high-power optical material," *SPIE Proceedings*, vol. 1275 (1990), pp. 2-9.
10. R. Seitz, "The end of the beginning," *SPIE Proceedings*, vol. 969 (1988), pp. 124-37.
11. J. Field, "Strength and fracture properties of diamond," in *The Properties of Diamond* (Academic Press, London/UK, 1979), Chap. 9.
12. D. Gray, ed., *American Institute of Physics Handbook* (McGraw-Hill Book Co., New York/NY, 1972).
13. M. Weber, ed., *CRC Handbook of Laser Science and Technology* (CRC Press, Boca Raton/FL, 1986), vol 4.
14. D. Jassowski, "Investigation of applications of diamond film," *Document no. AL-TR-89-044* (Aerojet Techsystems, Sacramento/CA, 1989).
15. T. Anthony, W. Banholzer, J. Fleischer, L. Wei, P. Kuo, R. Thomas, and R. Pryor, "Thermal diffusivity of isotopically enriched ^{12}C diamond," *Physical Review B*, vol. 42 (1990), pp. 1104-11.
16. M. Seal and W. von Enckevort, "Application of diamond in optics," *SPIE Proceedings*, vol. 969 (1988), pp. 144-52.
17. M. Yoder, "Artifact diamond: its allure and significance," *SPIE Proceedings*, vol. 969 (1988), pp. 106-13.
18. M. Thomas and R. Joseph, "Optical phonon charactistics of diamond, beryllia, and cubic zirconia," *SPIE Proceedings*, vol. 1326 (1990), pp. 130-6.

19. T. Hartnett and R. Miller, "Potential limitations for using CVD diamond as LWIR windows," *SPIE Proceedings*, vol. 1307 (1990), pp. 474-84.
20. S. Mitra and B. Bendow, eds., *Optical Properties of Highly Transparent Solids* (Plenum Press, New York/NY, 1975).
21. C. Klein, T. Hartnett, R. Miller, and C. Robinson, "Lattice vibrational modes and defect-activated IR absorptions in CVD diamond," *Proceedings of the Second International Symposium on Diamond Materials* (ECS, Pennington/NJ, 1991), in press.
22. J. Field, ed., *The Properties of Diamond* (Academic Press, London/UK, 1979), Appendix.
23. J. Turley and G. Sines, "The anisotropy of Young's modulus, shear modulus, and Poisson's ratio in cubic materials," *Journal of Physics D: Applied Physics*, vol. 4 (1971), pp. 264-71.
24. G. Simmons and W. Wang, *Single-Crystal Elastic Constants and Calculated Aggregate Properties: A Handbook*, (MIT Press, Cambridge/MA, 1971).
25. F. McClintock, ed., "Mechanical properties of infrared transmitting materials," *Document no. NMAB-336* (National Academy of Sciences, Washington/DC, 1978).
26. J. Rowe, A. Blume, and E. Boudreaux, "Dual-mode dome requirements for future air-to-air missiles," *Proceedings of the Third DoD Symposium on Electromagnetic Windows* (GACIAC, Chicago/IL, 1990), vol. 1, pp. 79-95.
27. A. Shapiro, *The Dynamics and Thermodynamics of Compressible Fluid Flow* (The Ronald Press Co., New York/NY, 1953), vol. 1.
28. S. Timoshenko and S. Woinowsky-Krieger, *Theory of Plates and Shells* (McGraw-Hill Book Co., New York/NY, 1959), chap. 16.
29. C. Klein, "Aerodynamic heating of hemispherical irdomes at supersonic speeds," *AIAA/ASME Thermophysics and Heat Transfer Conference* (Boston/MA, 1974); available as *Document no. T-844* (Raytheon Co., Waltham/MA).
30. C. Johnson and W. Weimer, "Optical properties of microwave-plasma-assisted CVD diamond film," *SPIE Proceedings*, vol. 1146 (1989), pp. 188-91.
31. R. Roark and W. Young, *Formulas for Stress and Strain* (McGraw-Hill Book Co., New York/NY, 1975), chap. 15.
32. H. Bennett, D. Burge, C. Lowe-Ma, and J. Bennett, "Optical properties of advanced infrared missile dome materials," *Document no. NWC-TP-6284* (Naval Weapons Center, China Lake/CA, 1981).
33. C. Klein, "Hot infrared domes: a case study," *SPIE Proceedings*, vol. 1326 (1990), pp. 217-30.
34. C. Klein, "Beam-induced spherical aberration in cooled CW laser light transmitting components," in *Laser-Induced Damage in Optical Materials: 1986* (USGPO, Washington/DC), pp. 96-126.
35. M. Abramowitz and I. Stegun, eds., *Handbook of Mathematical Functions with Formulas, Graphs, and Mathematical Tables* (USGPO, Washington/DC, 1964).

36. C. Klein, "Optical distortion coefficients of laser windows: one more time," *Optical Engineering*, vol. 29 (1990), pp. 343-50.
37. M. Born and E. Wolf, *Principles of Optics* (Pergamon Press, Oxford/UK, 1975), chap. 9.
38. R. Taylor and J. Goela. "Specification of infrared optical materials for laser applications," *SPIE Proceedings*, vol. 607 (1986), pp. 22-35.
39. P. Liu, R. Yen, and N. Bloembergen, "Dielectric breakdown threshold, two-photon absorption, and other optical damage mechanisms in diamond," *IEEE Journal of Quantum Electronics*, vol. 14 (1978), pp. 574-6.
40. M. Sparks and M. Cottis, "Pressure-induced optical distortion in laser windows," *Journal of Applied Physics*, vol. 44 (1973), pp. 787-94.